# AUTOMATED TARGET-FREE CAMERA CALIBRATION

**Clive S. Fraser**
**Christos Stamatopoulos**
Cooperative Research Center for Spatial Information
Dept. of Infrastructure Engineering
University of Melbourne, VIC 3010, Australia
c.fraser@unimelb.edu.au
xstamatopoulos@gmail.com

## ABSTRACT

Automatic camera calibration is now a well-established procedure. The process generally involves photographing a target array to form a network of images in a geometric configuration suited to self-calibration. Full automation can be implemented if coded targets are employed, as these provide initial image point correspondences necessary for network exterior orientation. While the use of coded and indeed any artificial targeting facilitates high accuracy recovery of camera calibration parameters, it is also fair to say that the employment of targets can be inconvenient in some practical circumstances, for example when attempting calibration from low-level aerial imagery, as with UAVs, or when calibrating long-focal length lenses where small image scales call for inconveniently large coded targets. Fortunately, accompanying the adoption of so-called structure-from-motion (SfM) approaches in photogrammetric network orientation, there is the prospect of fully automated camera calibration without the need for artificial targets. Instead of the image-point correspondence problem being overcome through the use of coded targets, feature-based matching is employed to provide the necessary point matches to support exterior orientation. Whereas it is not uncommon to achieve an accuracy of camera calibration of 0.1 pixel or better through the use of coded targets, the resolution from the feature-based matching process is generally closer to 0.3 pixel. This difference is offset, however, by the fact that whereas 100 or so targets might be employed, the SfM approach can easily involve 10,000 or more feature points on a feature-rich object, thus leading to a very comprehensive calibration result. This paper reports on the application of the SfM approach to automated target-free camera self-calibration and discusses the process via practical examples.

**KEYWORDS:** Camera Calibration, Target-Free Calibration, Feature-based Matching, Automatic Calibration, Structure from Motion

## INTRODUCTION

Automatic calibration of digital cameras used for photogrammetric measurement has now been a practical reality for close to two decades. Until relatively recently, however, the procedure for producing scene-independent calibration parameters for close-range photogrammetric applications has required the use of targets, and notably coded targets to facilitate automated initial image point correspondence determination. While targeting continues to be widely used, especially in high-accuracy industrial and engineering measurement where precise positioning of specific object points is central to many dimensional metrology tasks, the use of artificially signalized points and especially coded targets, is nevertheless inconvenient in an increasing number of applications. Two examples are networks of images captured from UAVs and measurements over longer distances with lenses of long focal length, the required coded targets being inconveniently large in both instances.

The adoption of Structure from Motion (SfM) algorithms from computer vision in multi-image photogrammetric orientation is becoming increasingly more popular as a means of solving the image point correspondence problem and providing preliminary network exterior orientation in the absence of targets (eg Barazetti et al., 2011a; Remondino et al., 2012; Wohlfeil et al., 2013; Alsadik et al., 2013). However, although there has been rapid adoption of SfM and multi-view stereo approaches in close-range photogrammetry, and especially in UAV applications, there has been less attention paid to the prospect of utilizing these same approaches for stand-alone camera calibration, though the prospect has been recognized (eg Barazzetti et al., 2011b; Stamatopoulos & Fraser, 2013). This paper examines the potential of fully automatic, targetless high accuracy camera calibration via a

process that combines SfM methods with rigorous photogrammetric orientation and self-calibration models. A perceived drawback of the SfM approach for close-range camera orientation is that it has difficulty accommodating convergent imagery due to the adoption of linear techniques and descriptor-based feature point matching. Yet, convergent imaging configurations are generally a prerequisite for reliable camera self-calibration and thus any multi-view stereo approach must accommodate wide as well as narrow baselines (image-to-image separation).

## DATA PROCESSING

As previously reported (Stamatopoulos et al., 2012; Stamatopoulos & Fraser, 2013), the authors have been developing a data processing pipeline for targetless automatic network orientation, which includes camera self-calibration. The first stage in the process is feature point detection, followed by pair-wise 2D image matching based on feature descriptors. The feature-point matching produces a significant percentage of outliers, which are then filtered out via geometric consistency checks, such as adherence to epipolar geometry and cluster analysis based on projective transformation (Stamatopoulos et al., 2012). A coplanarity-based automatic relative orientation of a selected image pair then follows, eg the pair with the most number of feature points matches or the most feature points matched to adjacent images. After this, the preliminary exterior orientation of the network is built through successive resections to establish camera station positions and orientations, and spatial intersections to determine initial 3D coordinates of matched feature points. Bundle adjustments with relaxed outlier rejection tolerances are also interspersed within this sequential multi-image network formation stage. The process culminates in a final bundle adjustment, with self-calibration of the camera(s) in instances where the network geometry affords the recovery of interior orientation and lens distortion parameters. An important attribute of the final bundle adjustment, especially in cases where high-accuracy (sub-pixel) results are required is that it provides rigorous quality measures in relation to precision and reliability for the parameters of both image and object space.

This data processing pipeline affords target-free exterior orientation of very large and complex photogrammetric networks, with the primary constraint upon its application being the requirement for a feature-rich object space. Objects satisfying the texture requirements are regrettably less common in vision-based industrial and engineering measurement, and thus we see SfM approaches being more suited to applications such as aerial triangulation, especially from UAVs, and in architectural and archaeological photogrammetry (eg Lucieer et al., 2012; Barazettti et al., 2011a, Wohlfeil et al., 2013). Regardless of the application, camera calibration remains a central component of photogrammetric measurement and new automated approaches to calibration that do not require targets are always worthy of evaluation.

## EXPERIMENTAL TESTING

### Network Configurations

The experimental testing phase involved the carrying out of three self-calibrations of two cameras. The first of the cameras was an off-the-shelf 10 mpixel Nikon D200 DSLR with a 17mm unifocal lens. The only concession made is regard to rendering this camera metric was to tape the lens barrel so as to ensure a fixed focus (of nominally 5m). The camera was to be hand-held within two multi-image, convergent close-range network configurations. The second camera was a Canon IXUS 100 IS consumer camera with an integrated zoom lens, with the focal length being set to 5.9mm. This camera was deployed within a UAV flying at a mean flying height of 200m in a 23-image block configuration of near-nadir imagery. The images used for the calibration testing of the Canon IXUS formed a sub-block of a larger network established to investigate the accuracy potential of DEM determination from UAV imagery (Cramer, 2013). This data set was kindly provided to the authors by the Institute for Photogrammetry at the University of Stuttgart.

In the case of the Nikon D200, two self-calibration networks were to be established, with there being a requirement that these would be suitable for automated exterior orientation via both coded targets and ‘natural’ feature points extracted via interest point detectors. As has been mentioned, it was anticipated that image measurement and correspondence determination to 0.1 pixel accuracy would be achieved in the targeted networks, where the image point correspondence determination is via the codes. On the other hand, an accuracy of close to 0.25 – 0.4 pixels was to be expected for the feature-based matching of ‘natural’ interest points, the correspondence

determination and filtering of feature points being in accordance with the widely adopted multi-view stereo approach of SfM, namely pair-wise descriptor-based matching.

The plan was to utilize the same imagery for the targeted and untargeted cases in the calibrations of the Nikon D200 camera, with the network geometry needing to support a camera parameter recovery of maximum fidelity. To maximize the prospects of recovering a scene independent calibration, while minimizing projective coupling between interior and exterior orientation parameters, the following geometric characteristics were adopted:

- A highly convergent imaging configuration comprising 20 or more camera stations, albeit with limited camera station separation in the vertical direction (only a short ladder was at hand!)
- A wide diversity of orthogonal roll angles
- An object that was three dimensional, such that the target and feature point fields were non-coplanar.
- An object with rich texture suited to interest point detection via operators such as SIFT and SURF. The artificial coded targets comprised simply printed 11mm-diameter white dots on a black background.

The two networks for the Nikon DSLR calibration are shown in Figures 1a and 2a. Both comprised sections of wall from two buildings, one of light sandstone, Figure 1a, which had had 160 years to weather. Here the texture was not 'rich', but moderate, however the texture on the brick paving in front of the wall proved to be very rich and, as it turned out, very favourable for feature point matching. There was also some vegetation, ivy, across the base of the 6m section of wall. The second building, Figure 2a, was red brick, and this exhibited moderate texture. Again, the brick paving in front of the 5m section of wall provided more feature points than originally anticipated, which enhanced to 3D nature of the object point array in the target-free calibrations.

The photogrammetric networks for the Nikon D200 calibration are shown in Figure 1b, for the sandstone building, and 2b, for the red brick building. In the former, 25 codes (200 points) and 24,500 feature points were recorded within the 27 images (each point seen in a minimum of 4 images). In the latter, 31 images covered 24 codes (192 points) and 13,300 feature points. In both cases the set-back distance from the target array was approximately 5.5m, leading to an average image scale of 1: 300.

In the case of the UAV network, a vineyard area of approximately 320 x 250 m with a height range of 60m was imaged in a configuration of three strips of nominally 90% forward and 70% side overlap, with an additional cross strip, captured at an image scale of close to 1:33,000 (GSD of 5cm) . The configuration of the 23-image block is shown in Figure 3. The scene was feature-rich, with some 20,000 feature points being matched, the number of imaging rays per matched point varied from a maximum of 19 down to an assigned minimum of four.

## Self-Calibration Adjustments

SfM approaches to 3D shape and camera pose determination in multi-view stereo networks often imply the application of linear algorithms and camera 'calibrations' which are neither metrically precise, scene independent nor image invariant. This was not the case here. The SfM approach was utilized only for the feature-point correspondence determination and outlier detection (via RANSAC and the fundamental matrix) within the pair-wise image matching. As mentioned, once the correspondences had been established, the process reverted to a standard, rigorous and fully automatic photogrammetric processing pipeline comprising an initial single-pair relative orientation, followed by iterative resection/intersection/bundle adjustment computations to build the preliminary network exterior orientation. This was followed by a final bundle adjustment with full self-calibration and covariance propagation of network parameters to afford comprehensive quality assessment. The software utilized for all stages of the image measurement and self-calibrations was *iWitnessPRO* (Photometrix, 2014) for the untargeted cases and *Australis* (Photometrix, 2014) for the networks with coded targets. Not surprisingly, the processing of the networks of 200-odd targets and 30 or so images was much faster than in the untargeted cases, the full computation time being under 1 minute. This is against the time taken for the untargeted networks, which was 20 and 17 minutes, respectively, for the Sandstone and Brick Wall networks, and 11 minutes for the 23-image, 20,000 point UAV network. Of course when one adds in the 10-15 minutes required to affix the coded targets, there is not a great deal of difference in the overall time involved for the two Nikon D200 calibration approaches.

(a)

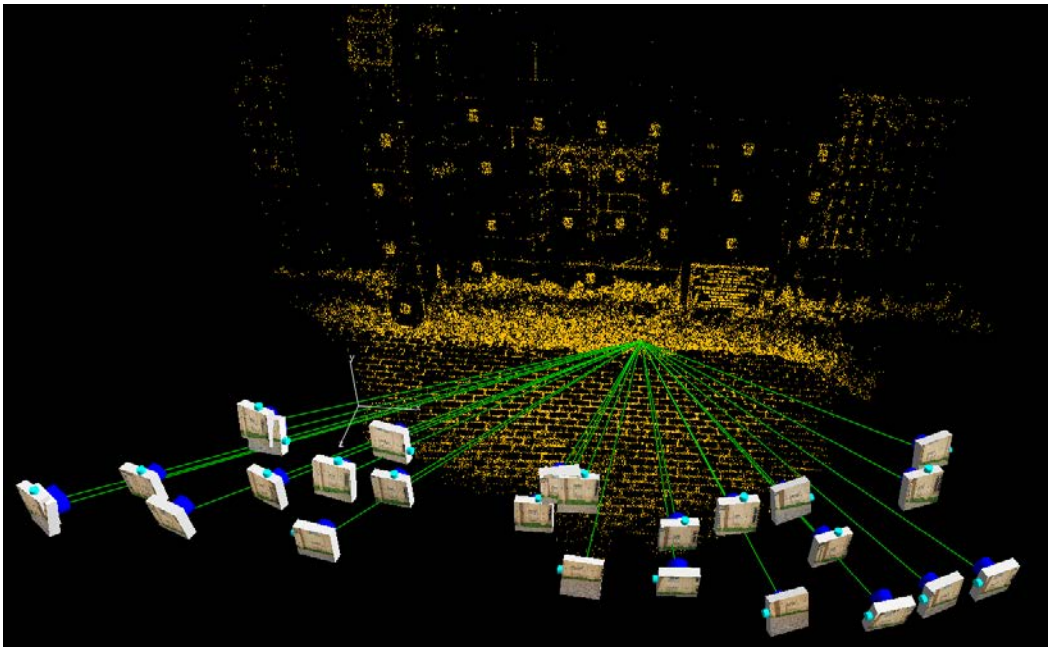

(b)

**Figure 1.** Configuration for 25,000 point ‘Sandstone’ self-calibration network for Nikon D200 SLR.

(a)

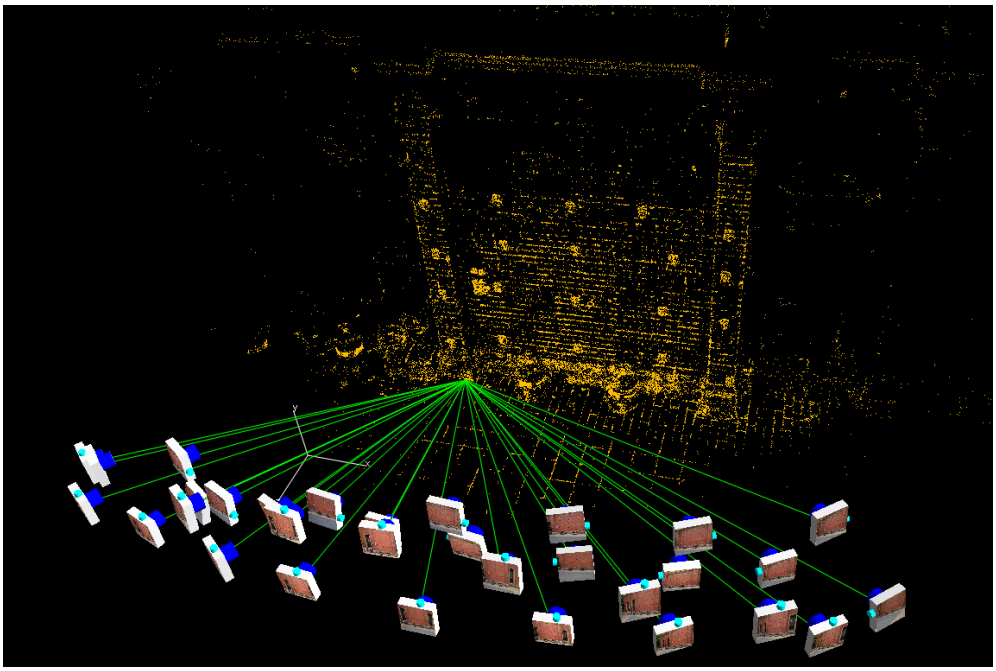

(b)

**Figure 2.** Configuration for 13,500 point 'Brick Wall' self-calibration network for Nikon D200 SLR.

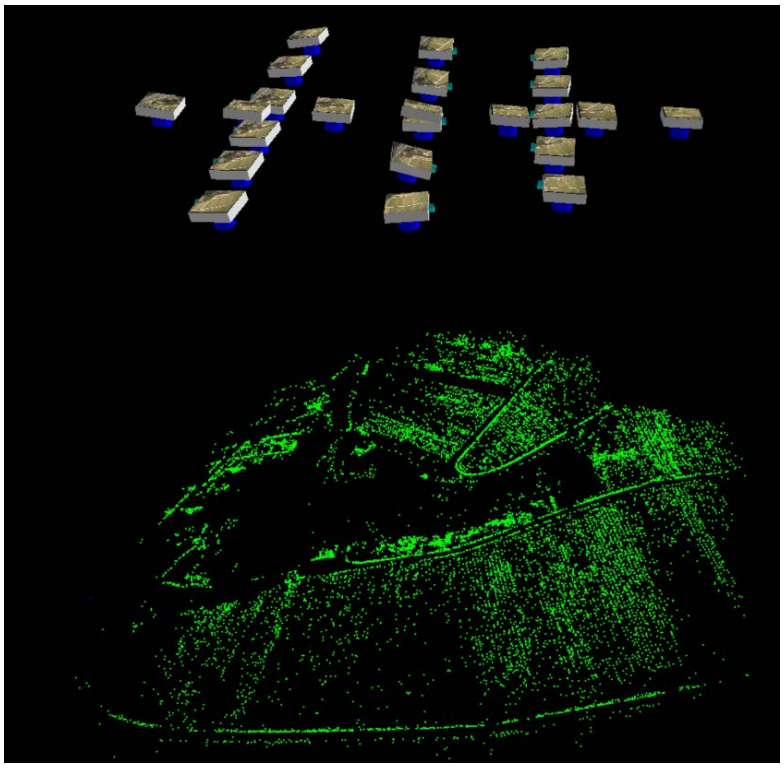

**Figure 3.** Configuration for 20,000 point Hessigheim UAV self-calibration network for the Canon IXUS 100 IS.

# RESULTS

## Nikon D200 Calibrations

Table 1 provides a summary of the results of the self-calibrating bundle adjustments for the two Nikon D200 networks. Listed are the adjusted values of the interior orientation parameters, focal length c, and principal point offsets $x_p$, $y_p$, along with their estimated standard errors. Also listed are radial distortion correction values at three selected radial distances and two decentring distortion profile values listed for two radial distances. The reason for reporting lens distortion in this manner is that it provides a more easily interpretable indicator of the repeatability of the computed distortion profiles than would be the case if polynomial coefficients only were listed. The RMS value of image coordinate residuals and the number of object points in each network adjustment are also shown in the table.

Two aspects of the results listed in Table 1 are worthy of note prior to any discussion of the quality of the camera self-calibrations. The first is that in view of the fact that the Nikon D200 could not be considered a truly metric camera, given that no effort had been made to stabilise the lens assembly, the expectations of high repeatability in interior orientation parameters between the two networks should not be too high. However, expectations of repeatability between the targeted and untargeted cases, which used the same images, should be high. The second point to recall here is that we do not know the 'true' calibration values, and the quality and fidelity of the self-calibrations can only be assessed via internal means. Here, two measures are effectively relied upon, namely the precision and repeatability of recovery of the calibration parameters, and the resulting discrepancies in object space coordinates when these parameters are subsequently applied. In the following paragraphs the former measure is discussed, whereas the latter measure will be addressed in the following section.

**Table 1**. Results of self-calibrations of the Nikon D200 camera for targeted and untargeted cases.

| | Focal length, c ($\sigma_c$) mm | $x_p$ ($\sigma_{xp}$) mm | $y_p$ ($\sigma_{xp}$) mm | $\Delta$r @ r=8mm µm | $\Delta$r @ r=10mm µm | $\Delta$r @ r=12.0mm µm | P(r) @ r=10mm µm | P(r) @ r=12mm µm | RMS $v_{xy}$ No of points |
|---|---|---|---|---|---|---|---|---|---|
| **Sandstone** | | | | | | | | | |
| Coded targets | 17.632 (0.0011) | -0.040 (0.0008) | -0.193 (0.0008) | 121.7 | 217.3 | 333.2 | 5.7 | 8.1 | 0.34 pl 24,500 |
| Untargeted | 17.620 (0.0007) | -0.040 (0.0004) | -0.192 (0.0004) | 121.6 | 217.5 | 334.8 | 5.2 | 7.5 | 0.10pl 200 |
| **Brick Wall** | | | | | | | | | |
| Coded targets | 17.621 (0.002) | -0.084 (0.002) | -0.199 (0.003) | 122.7 | 218.1 | 333.2 | 6.2 | 8.9 | 0.14pl 192 |
| Untargeted | 17.634 (0.0004) | -0.054 (0.0001) | -0.191 (0.0001) | 121.4 | 216.9 | 333.8 | 5.7 | 8.1 | 0.28pl 13,300 |

Salient points from the self-calibrations, summarized in Table 1, are as follows:

- As anticipated, there is a 2 – 3 times discrepancy between the accuracy of image coordinate measurement in the targeted and untargeted cases, with the RMS $v_{xy}$ values being close to 0.1 pixel for the targeted cases and 0.3 pixels for the feature-based matching cases. It is interesting to note that there were no common points between the two cases. Although the same images were used, none of the coded target 'dots' were extracted by the interest point detectors. On the basis of the difference in triangulation closure alone, it could be anticipated that the precision of recovery of calibration parameters would be better for the targeted case.
- The precision of recovery calibration parameters was in fact superior for the untargeted network adjustments, simply because there were so many more multiply matched feature points than coded targets, there being more than 60 untargeted points for every artificial target. From a practical point of view, this is a noteworthy finding because it illustrates that the feature-based matching approach coupled with very dense point fields of thousands of points can yield camera calibration parameters to higher precision than from targeted arrays comprising a few hundred points. The same phenomenon was experienced with the development of image matching-based relative orientation on photogrammetric workstations back in the 1990s (eg Heipke, 1996)
- The repeatability between the targeted and untargeted cases was very high for the lens distortion parameters and high for the interior orientation elements in the Sandstone network, being to within 1 µm (0.16 pixel) for all values listed, other than the principal distance. The repeatability of interior orientation parameters is lower for the Brick Wall network, though still within practical expectations. A possible reason for the higher camera parameter discrepancies found in the Brick Wall network may be that the image points for the untargeted case covered a significantly greater area of image format than for the targeted case and thus the radially dependent lens distortion functions were modelled with greater fidelity and the scale variation within images in the untargeted network was greater, which is a desirable attribute for self-calibration networks employing highly convergent imaging configurations.
- On the subject of convergent imaging, there was one noteworthy surprise. Whereas it could be anticipated that accurate centroiding on high-contrast circular targets would be possible to incidence angles of 30 degrees to the target plane and potentially lower, there was not the same level of confidence that descriptor-based matching of feature points would accommodate moderately high convergence angles. This would

suggest that the imaging geometry of the targeted array might be stronger, due to points having a higher number of imaging rays over a wider diversity of viewing angles. However, as indicated in Figures 1b and 2b, it turned out that the feature based matching could accommodate relatively wide baselines, resulting in many points having effective convergence angles between imaging rays of up to 90 degrees. The success with the multi-ray matching of features also resulted in object point arrays which were better distributed in three dimensions than the targeted arrays.

## Quality in Object Space

In order to assess the impact on object space point determination of the variation in the calibration parameters computed in the untargeted and targeted cases for the Nikon D200, a simple test was carried out. From the two sets of 30-odd images, two subsets were selected, 10 from the Sandstone and eight from the Brick Wall data set. Standard bundle adjustments employing the camera parameters from the self-calibrations were then carried out for each of these networks, the aim being to determine the accuracy of object point determination - for the coded targets only - as quantified by the XYZ coordinate discrepancies. The two networks are shown in Figure 4, where it can also be seen that the array of coded targets was used. Listed in Table 2 are the RMS values of XYZ object point coordinate standard errors obtained in the network adjustments. These show anticipated accuracies (RMS 1-sigma) of 0.13 to 0.18 mm in the depth direction (Z), and between 0.05 and 0.08 mm in the dominant plane of each target array (XY). There is little distinction in quality as judged by the RMS $v_{xy}$ values. In the Sandstone network, the triangulation closure is marginally better for the calibration obtained from the coded targets (Cal. 1 in Table 2), and in the Brick Wall network the calibration obtained from the feature-based matching (Cal. 2 in Table 2) yields a lower RMS $v_{xy}$ value of 0.08 pixel. On the basis of RMS $v_{xy}$ values there is minimal distinction between the four network adjustments, and thus by implication no practical difference between the four camera calibrations.

A further means to assess calibration quality is via an examination of the difference in the computed shape of the object point fields determined from the different sets of calibration parameters, for both the Sandstone and Brick Wall test fields. The computed RMS coordinate discrepancy values are listed in Table 2, where it can be seen that the overall agreement in coordinate determination is at the level of 0.14mm or 1:40,000 of the size of the object field for the Sandstone network, and 0.16 or 1:25,000 for the Brick Wall network. This impressive level of agreement is reasonably consistent with standard error estimates based on the coordinate precision listed in Table 2. Nevertheless, it is interesting to note that the differences in object point XYZ coordinates obtained with the different camera calibration parameter sets show clearly systematic trends. This is illustrated in Figure 5, where the coordinate differences for the coded target clusters of 8 individual targets show consistent magnitude and orientation.

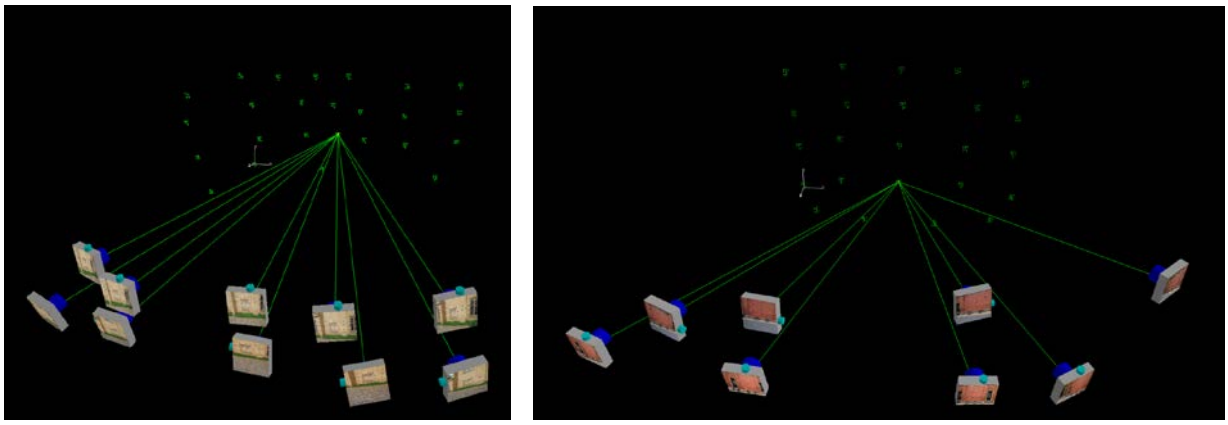

(a) Sandstone 10-image network (b) Brick Wall 8-image network

**Figure 4**. Photogrammetric networks used to assess camera calibration results.

**Table 2**. Object point precision and coordinate discrepancies for adjustments run with different calibration parameter sets.

| | Object Point Standard Errors (mm) | | | RMS $v_{xy}$ |
|---|---|---|---|---|
| **Sandstone** | $\sigma_X$ | $\sigma_Y$ | $\sigma_Z$ (depth) | pixels / µm |
| Cal. 1 (targets) | 0.065 | 0.081 | 0.152 | 0.08 / 0.49 |
| Cal. 2 (FBM) | 0.072 | 0.067 | 0.177 | 0.09 / 0.54 |
| **Brick Wall** | | | | |
| Cal. 1 (targets) | 0.064 | 0.065 | 0.146 | 0.09 / 0.56 |
| Cal. 2 (FBM) | 0.056 | 0.057 | 0.129 | 0.08 / 0.50 |
| | RMS coordinate discrepancy values: Cal. 1 versus Cal. 2 (mm) | | | |
| | $S_X$ | $S_Y$ | $S_Z$ (depth) | $S_{XYZ}$ |
| Sandstone | 0.11 | 0.06 | 0.20 | 0.14 (1:40,000) |
| Brick Wall | 0.17 | 0.16 | 0.14 | 0.16 (1:25,000) |

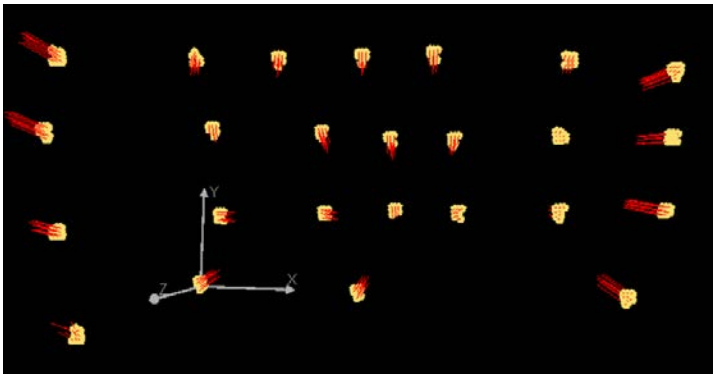


(a) Sandstone point field

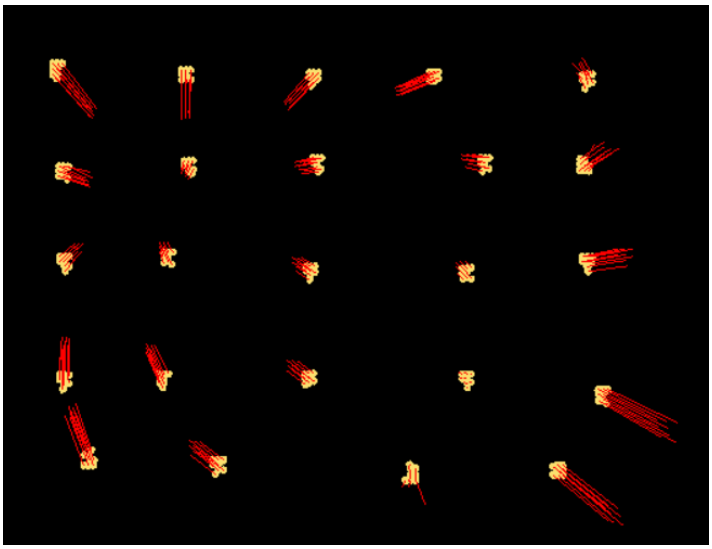

(b) Brick Wall point field

**Figure 5**. Object point discrepancies from network solutions using different calibration parameter sets.

## Canon IXUS in UAV Image Network

The scope of assessing the self-calibration of the Canon IXUS 100 IS employed in the network of 23-images recorded from a flying height of 200m with a small fixed-wing UAV was quite limited. The camera had been pre-calibrated and the images resampled to a distortion-free state (which included a correction for principal point offset). Thus, the success of the untargeted, feature-based matching approach could be partly assessed by how close the parameters recovered for radial distortion and principal point offset were to zero.

Cramer (2013) has previously reported on the accuracies obtained in bundle adjustment and subsequent DEM generation within a larger network of the same Canon IXUS imagery that is considered here, although the present investigation has been confined to a sub-block of 23 images. Some 20,000 feature points were used in the self-calibrating bundle adjustment of this network, with all points being matched across three or more image pairs. With the high forward and side overlap within the block, complemented by the cross strip, it was found that more than 100 points were successfully matched across 15 or more image pairs, which augured well for a successful recovery of the camera parameters. However, the authors did not have access to camera station GPS information and thus accurate focal length recovery was precluded.

Given the high projective coupling between decentring distortion and principal point offset in the network of near-nadir imagery, decentring distortion coefficients were also suppressed in the self-calibration. Object point precision varied dramatically between feature points, ranging from a mean standard error value of 4mm for 18-ray points to 12 cm for some 4-ray points. The overall RMS $v_{xy}$ value was 0.37 pixels and the RMSE from the fit to 6 GCPs was 2.1cm (better than half the 5cm GSD). As regards the recovered camera calibration parameters, $x_p$ and $y_p$ values of -4 and 1μm, respectively, were obtained and the recovered radial distortion profile did not exceed 0.5 μm or 0.3 pixel throughout the working format of the lens. The fact that these values did not significantly depart from zero, coupled with the internal quality measures from the bundle adjustment provided sufficient validation of the success of the target-free calibration of the Canon IXUS camera.

## CONCLUDING REMARKS

The target-free camera calibration tests conducted for the Nikon D200 and Canon IXUS 100 IS cameras have demonstrated that the SfM, feature-based matching approach to solving the image point correspondence problem, coupled with automated photogrammetric network orientation, can yield camera calibration parameters of greater precision and of equal accuracy, as far as could be assessed, to today's 'standard' automatic self-calibration approach which involves the use of targets. The poorer image point measurement accuracy of descriptor-based feature point matching is more than offset by the provision of potentially 100-fold more object points within the photogrammetric network. Moreover, the test results from the Nikon D200 calibrations demonstrate that the approach can accommodate the convergent imaging configurations that characterise moderate-to-high accuracy close-range photogrammetric measurement, and which are necessary for reliable self-calibration. Within the close-range measurement context, both approaches fit well into automatic data processing pipelines, as exemplified by the *iWitnessPRO* software system, which accommodates both the targeted and targetless cases. Also, from a practical standpoint, if the scene or object being imaged is texture rich and conducive to the target-free approach, then this is arguably the more flexible automated camera calibration option, yet there is limited time distinction between the two processes since the time to position 50 or so coded targets to form an object point array, can be similar to the extra computation time associated with the target-free calibration.

## REFERENCES


Alsadik, B., Remondino, F., Menna, F., Gerke, M., Vosselman, G., 2013. Robust extraction of image correspondences exploiting the image scene geometry and approximate camera orientation. *Int. Arch. Photogramm. Remote Sens. Spatial Inf. Sci.*, Vol. XL-5/W1, 7 pages.

Barazzetti, L., Remondino, F. & Scaioni, M., 2011a. Automated and accurate orientation of complex image sequences. *International Archives of the Photogrammetry, Remote Sensing & Spatial Information Sciences*, Trento, Vol. XXXVIII-5 /W16, pp. 277-284.

Barazzetti, L., Mussio, L., Remondino, F. & Scaioni, M., 2011b. Targetless camera calibration. *International Archives of the Photogrammetry, Remote Sensing & Spatial Information Sciences*, Trento, Vol. XXXVIII-5 /W16, pp. 335-342.

Cramer, M., 2013. The UAV@LGL BW project – a NMCA case study. *Proceedings of Photogrammetric Week '13* (Ed. D. Fritsch). Wichmann, pp. 165-179

Heipke C., 1996. Automation of interior, relative and absolute orientation. *International Archives of Photogrammetry & Remote Sensing*, Vienna, XXXI(B3): 297-311.

Photometrix, 2014. http://www.photometrix.com.au [Accessed: 11 Feb. 2014].

Lucieer, A., Robinson, S., Turner, D., Harwin, S., Kelcey, J., 2012. Using a micro-UAV for ultra-high resolution multi-sensor observations of Antarctic moss beds, *Int. Arch. Photogramm. Remote Sens. Spatial Inf. Sci.*,Vol. XXXIX-B1, pp. 429-433.

Remondino, F., Del Pizzo, S., Kersten, T., Troisi, S., 2012. Low-cost and open-source solutions for automated image orientation – A critical overview. *Proc. EuroMed 2012 Conference, LNCS 7616*, pp. 40-54.

Stamatopoulos, C., Fraser, C. S., 2013. Target-free automated image orientation and camera calibration in close-range photogrammetry. *ASPRS Annual Conference*, Baltimore, Maryland, March 24-28, 8 Pages.

Stamatopoulos C, Chuang T.Y., Fraser C.S. & Lu Y.Y., 2012. Fully automated image orientation in the absence of targets. *Int. Arch. Photogramm. Remote Sens. Spatial Inf. Sci.*, Vol. XXXIX-B5, pp. 303-308.

Wohlfeil, J., Strackenbrock, B., and Kossyk, I., 2013. Automated high resolution 3D reconstruction of cultural heritage using multi-scale sensor systems and semi-global matching, *Int. Arch. Photogramm. Remote Sens. Spatial Inf. Sci.*, XL-4/W4, pp. 37-43.